Science Advances
AAAS

advances.sciencemag.org/cgi/content/full/5/8/eaav9308/DC1

Supplementary Materials for

Precise nanofiltration in a fouling-resistant self-assembled membrane with water-continuous transport pathways

Xunda Feng, Qaboos Imran, Yizhou Zhang, Lucas Sixdenier, Xinglin Lu, Gilad Kaufman, Uri Gabinet, Kohsuke Kawabata, Menachem Elimelech, Chinedum O. Osuji*

*Corresponding author. Email: cosuji@seas.upenn.edu

Published 9 August 2019, *Sci. Adv.* **5**, eaav9308 (2019)
DOI: 10.1126/sciadv.aav9308

This PDF file includes:

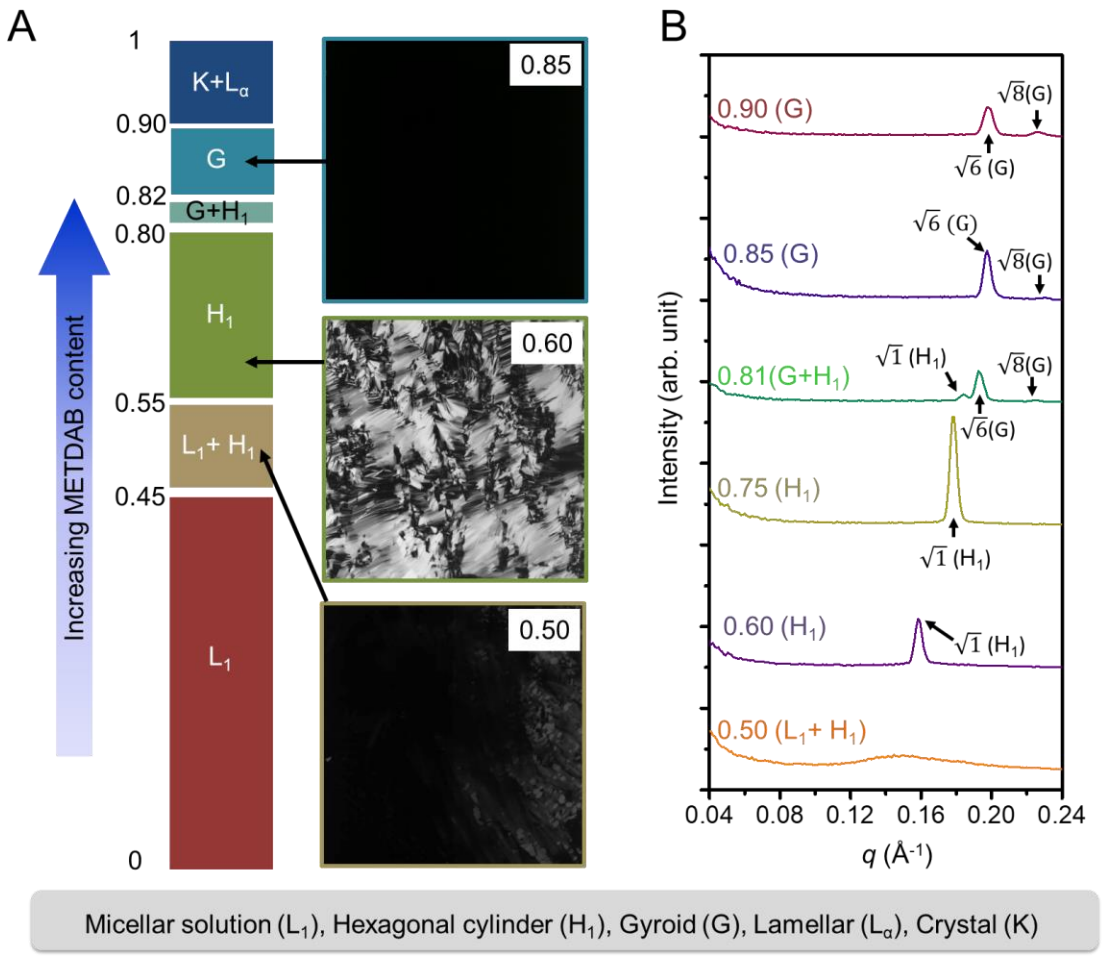

Fig. S1. METDAB/water binary phase diagram as determined by POM and x-ray scattering. The weight concentrations of METDAB are shown in the phase diagram. As the concentration of METDAB was increased, the surfactant/water mixtures followed a phase sequence of micellar solution (L_1), hexagonal cylinder (H_1), gyroid (G), lamellar (L_α), and crystal (K). Selective (A) POM images and (B) X-ray scattering data represent this sequence.

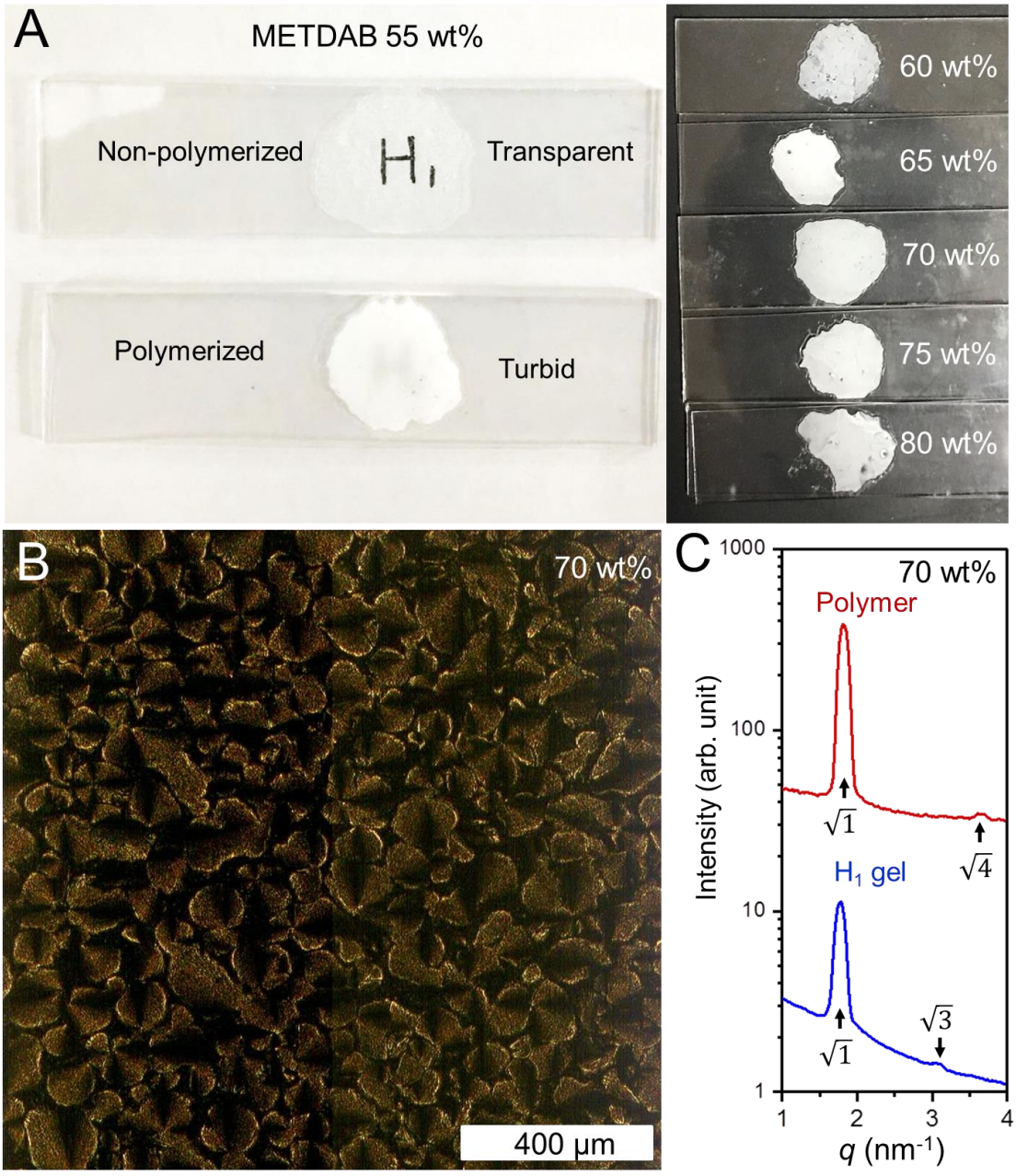

Fig. S2. Polymerization of H_1 mesophases formed by METDAB/water binary systems in the absence of cross-linkers. (A) Photos showing remarkable cloudiness in polymerized H_1 samples with different METDAB contents ranging from 55 to 80 wt%. (B) POM image of the polymerized H_1 mesophase with 70 wt% METDAB shows loss of the typical LC texture. (C) 1-D SAXS data displays that the ratio of peak locations changes from 1: √3 to 1: √4 after polymerization, indicative of disruption of the H_1 morphology. Photo credit: Xunda Feng, Yale University.

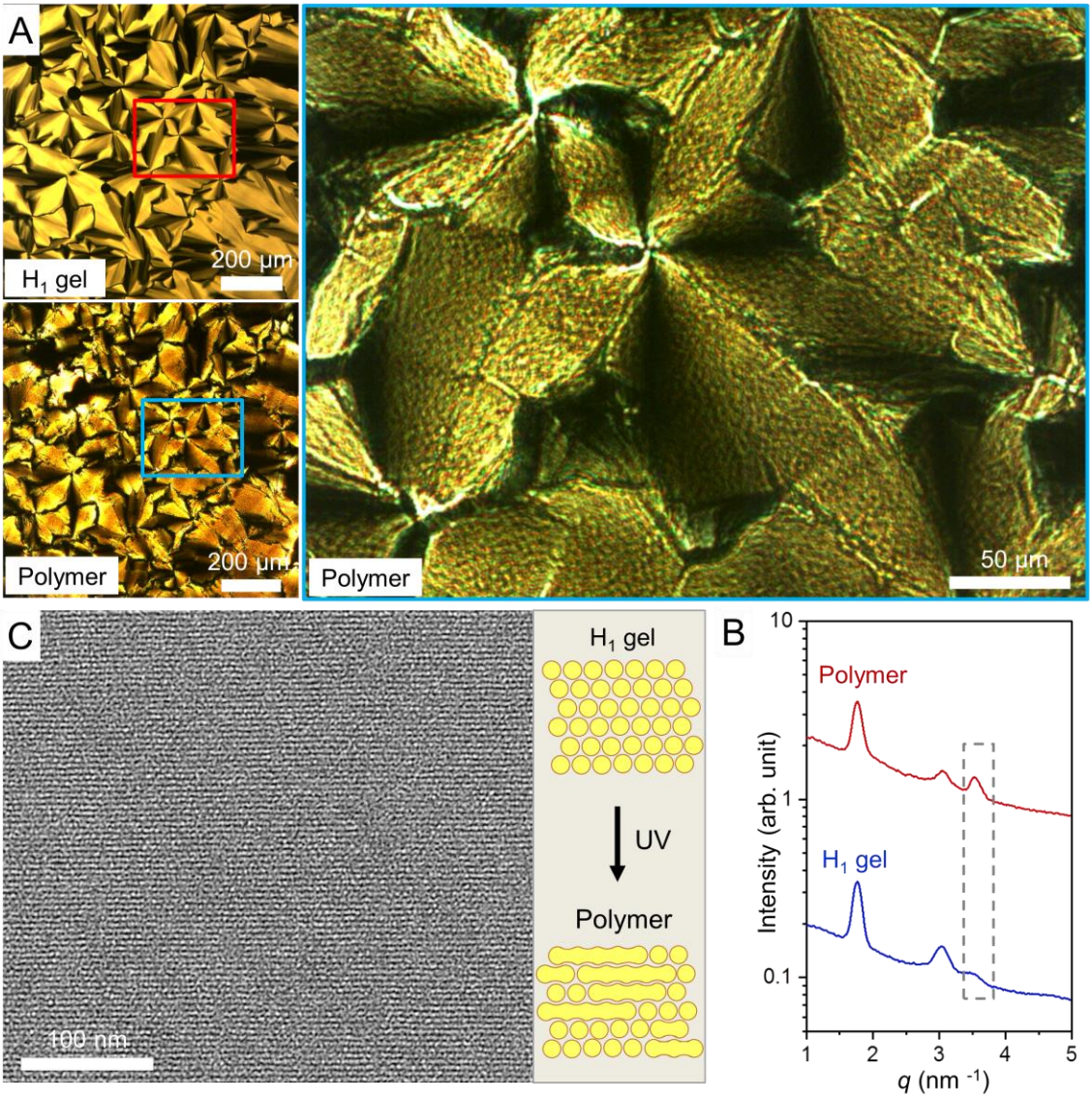

Fig. S3. Structural characterization of an H_1 mesophase containing only one cross-linking species in the hydrophobic core of cylindrical micelles before and after UV-initiated cross-linking. The cross-linker is 1,6-hexanediol dimethacrylate (HDMA). The mesophase contained 70 wt% METDAB, 6 wt% HDMA, and 24 wt% water. (A) Characteristic developable domain texture of the H_1 mesophase observed using POM before crosslinking. After UV induced cross-linking, a superficially similar, but discernably different, birefringent texture was observable in low magnification POM images. A magnified view (right) more clearly shows the emergence of optical inhomogeneities within the developable domains, reflecting disruption of the original H_1 morphology. Rectangles highlight the change of the LC texture induced polymerization. (B) X-ray scattering data showing intact peak locations but an unexpected increase of the intensity of the (200) peak after UV-induced cross-linking. (C) TEM image and schematic, illustrate the tendency of the hexagonal cylinders to transform to lamellar structures after cross-linking.

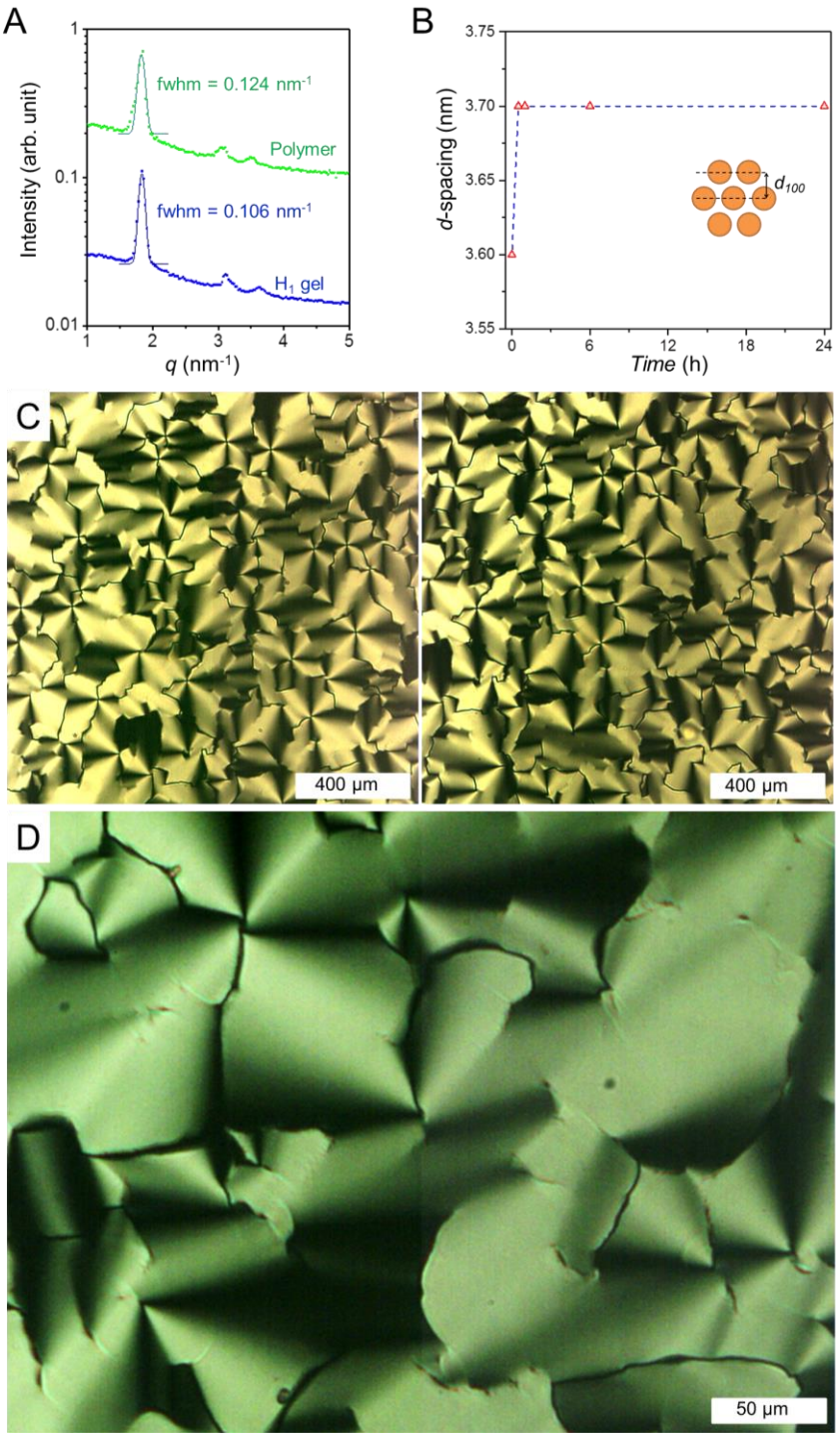

Fig. S4. X-ray scattering and POM data showing slight structural changes in the H_1 gel, the cross-linked H_1 mesophase, and the swelled polymer. (A) Gaussian fits of the (100) SAXS peaks of the H_1 gel and the corresponding polymer to obtain the values of full width at half maximum (fwhm). (B) Time dependent d_{100} spacing of the cross-linked H_1 membrane immersed in water as determined by X-ray scattering. (C) Low-magnification and (D) High-magnification POM images of the crosslinked H_1 mesophase.

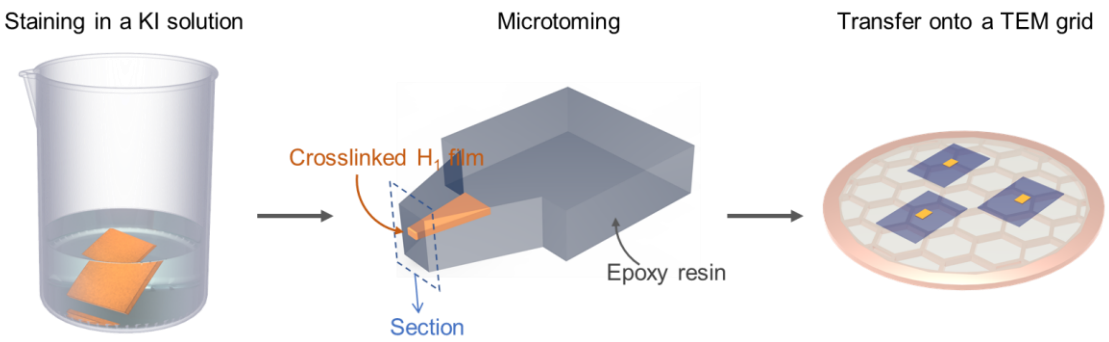

Fig. S5. Schematic illustration for the preparation of TEM samples.

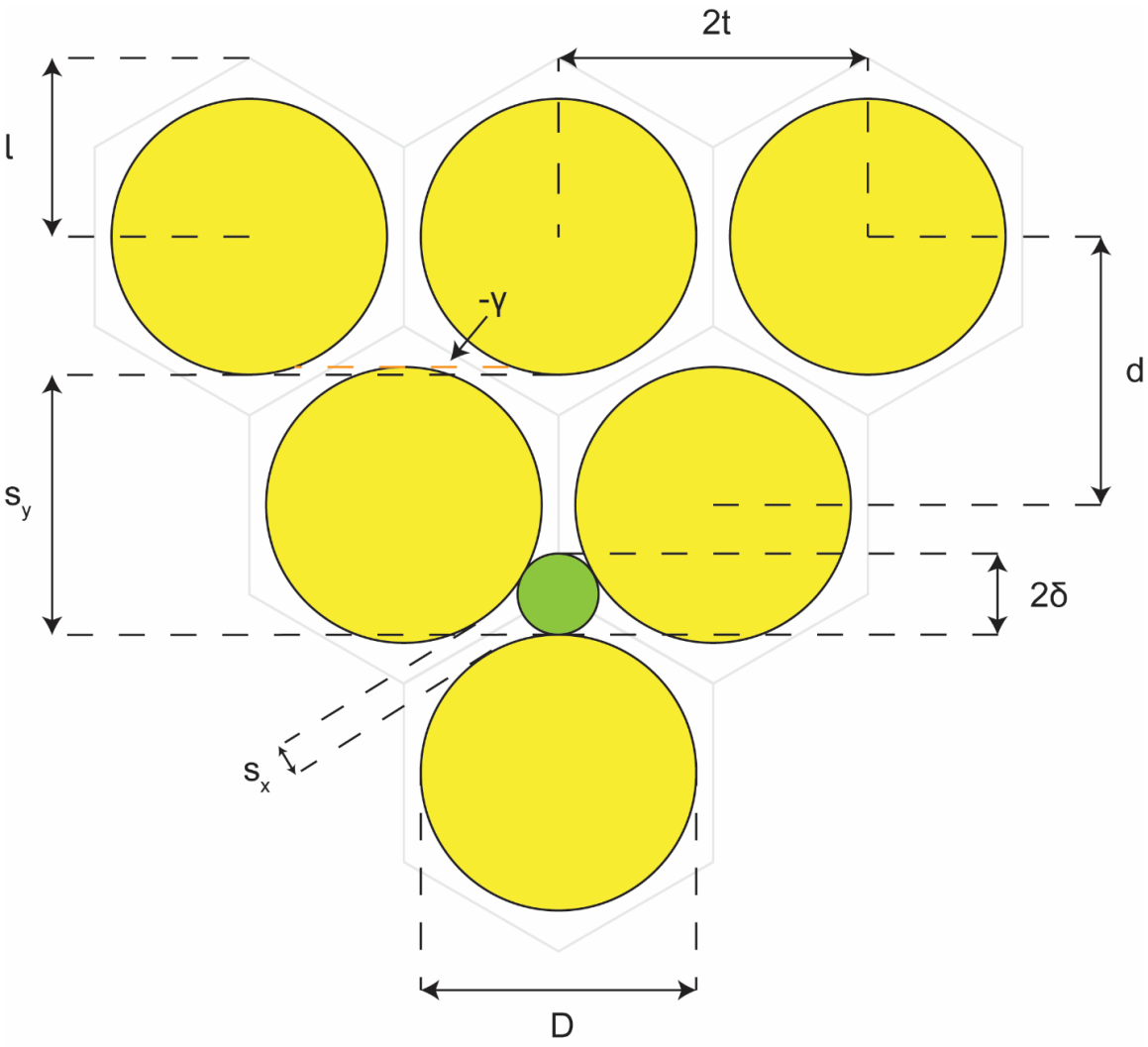

Fig. S6. Schematic illustration of the pore dimensions. The controlling dimensions of the structure are ~ 1.1 nm (2 δ) for transport in parallel and ~ 0.5 nm (S_x) for transport in perpendicular. Calculations are detailed in Section S1.

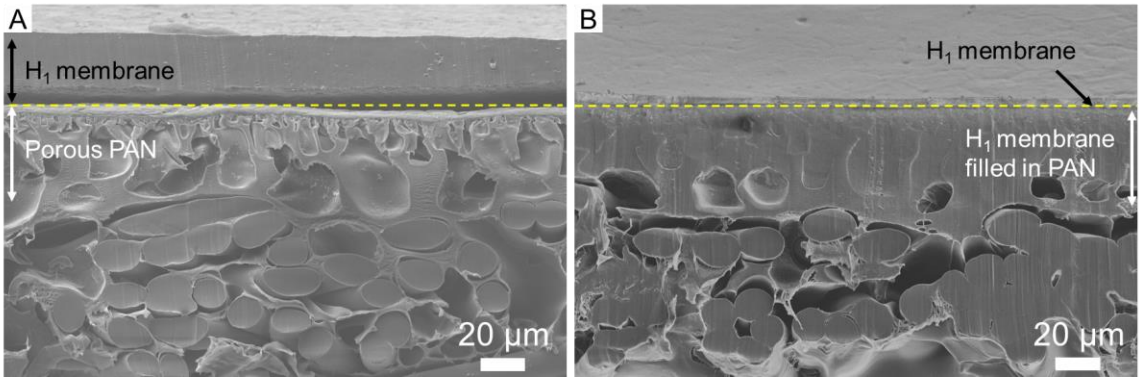

Fig. S7. SEM images showing the cross sections of the H_1/PAN composite membranes. The H_1 gel infiltrates the pores of the PAN support membrane during the pressing stage and the infiltrated H_1 is eventually crosslinked along with the surface H_1 layer.

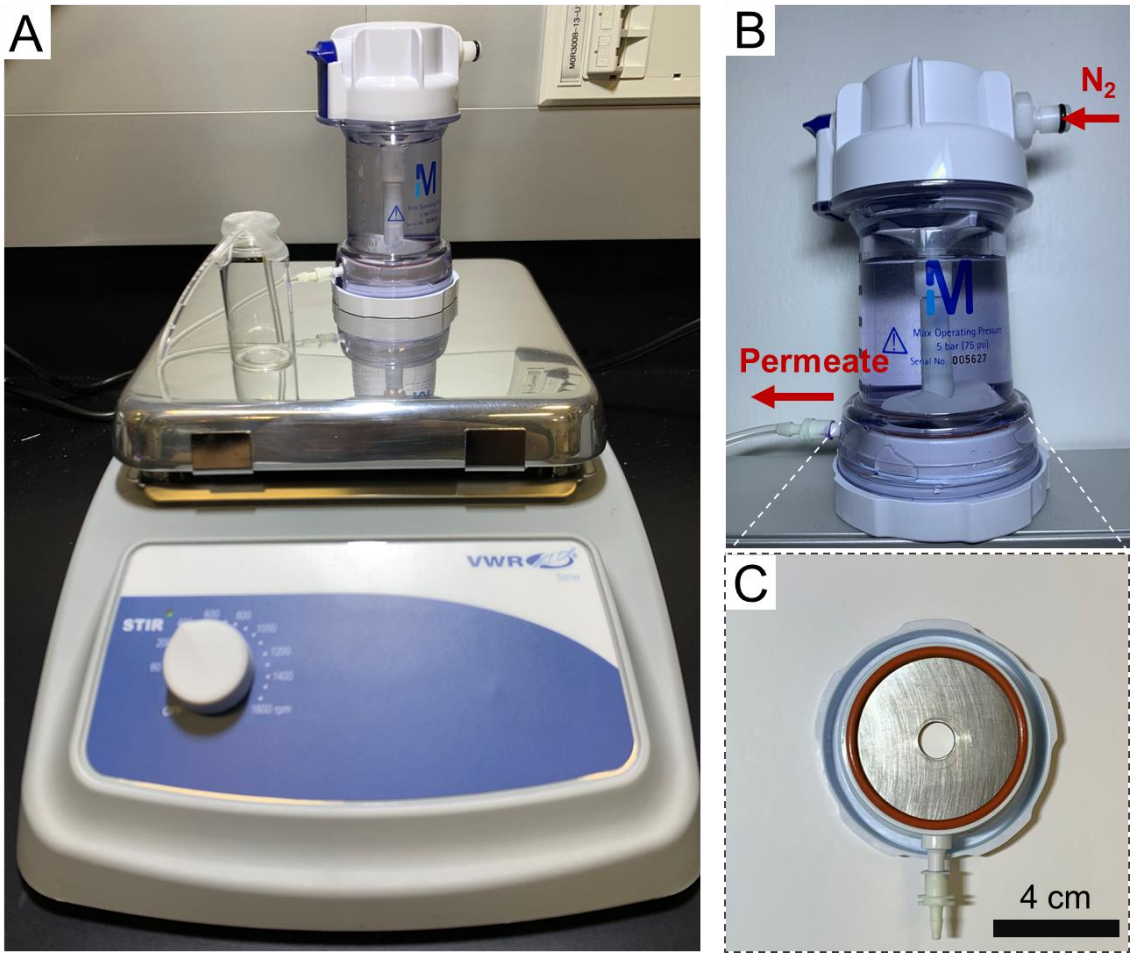

Fig. S8. Photos showing the stirred cell used for the nanofiltration test. (A) 50 mL EMD Millipore Amicon (UFSC05001) stirred cell. A stirring speed of 400 rpm was employed. (B) Photo showing the inlet of the compressed N_2 and the outlet of the permeate. (C) The active testing area of the membrane coupon was a circular area with a diameter of 1.1 cm. Photo credit: Yizhou Zhang, University of Pennsylvania.

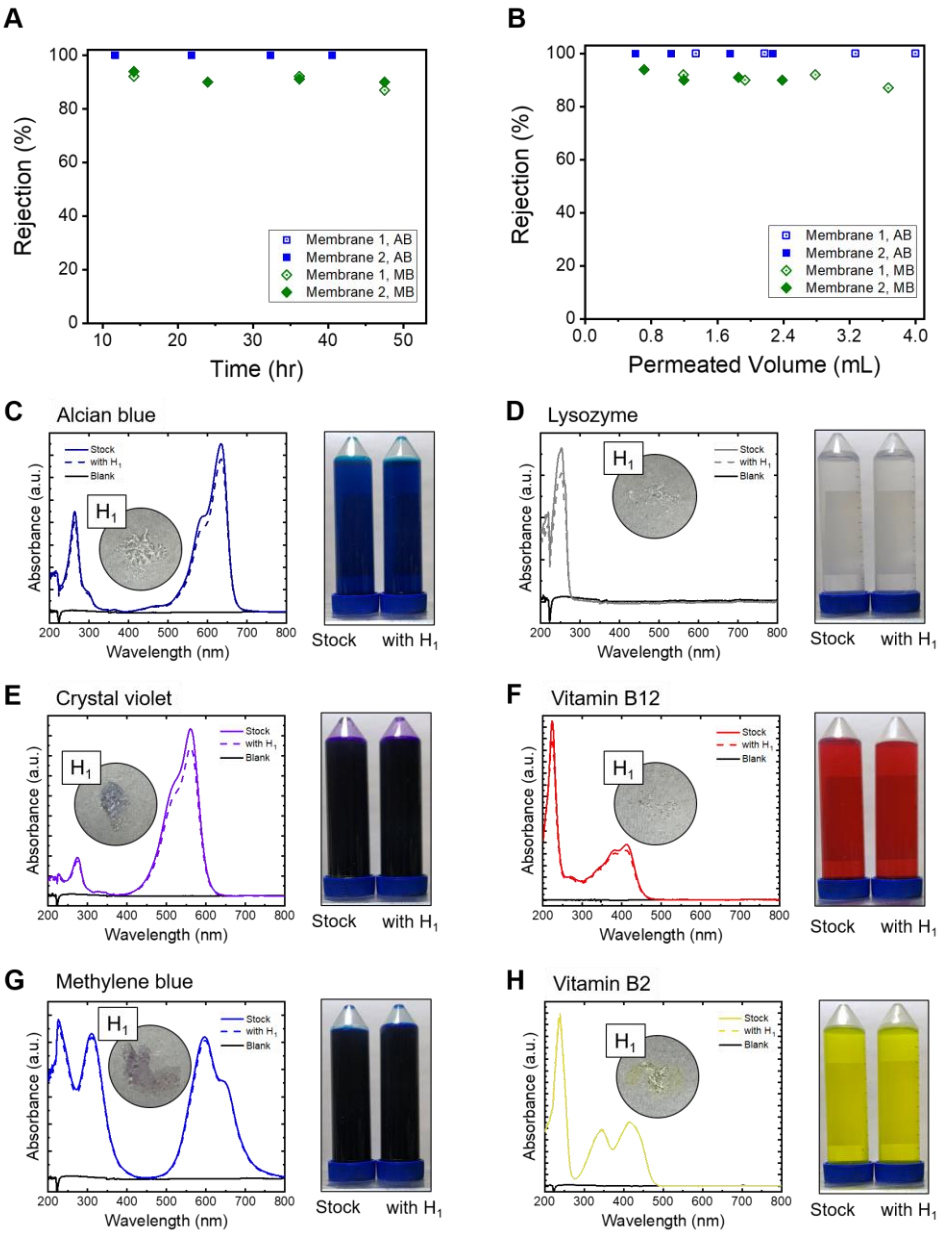

Fig. S9. The time-dependent solute rejection for H_1 composites and the static solute adsorption experiment for free-standing H_1 membranes. The time-dependent solute rejection tests suggest the separation performance of H_1 composite is independent of (A) experiment time and (B) permeated solution volume. UV-Vis spectroscopy was employed to determine the possible adsorption of dye molecules by the membranes. Dyes tested were (C) Alcian blue, (D) lysozyme, (E) crystal violet, (F) vitamin B_{12}, (G) methylene blue and (H) vitamin B_2. The experiment was performed with a same initial solute concentration as utilized during single solute rejection experiment, with a packing ratio of ~0.2 g membrane per L solution. The membranes did not uptake a significant amount of solute during prolonged soaking, suggesting adsorption did not affect the results in single solute rejection experiments. Photo credit: Yizhou Zhang, University of Pennsylvania.

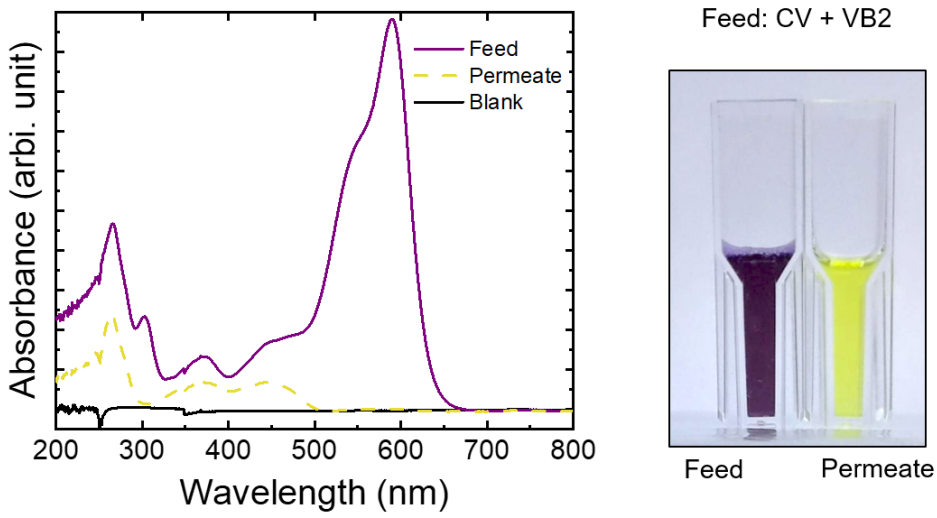

Fig. S10. UV-Vis spectrum and photographs demonstrating the competitive solute separation of CV and VB2. The membrane selectively rejects CV while allowing VB2 to partially permeate through (R ~ 50%). Photo credit: Yizhou Zhang, University of Pennsylvania.

Section S1. Calculation of the pore dimensions in an H_1 membrane

As simply illustrated in fig. S6, the geometry of an H_1 membrane consists of a continuous water transport path and discontinuous cylinders (colored in yellow). The volume fractions of the cylinders ϕ and the water transport path 1-ϕ are assumed to be 0.72 and 0.28, respectively, on the basis of the original composition of the H_1 gel. The distance of the neighboring (100) planes d was determined by X-ray scattering to be 3.6 nm.

$$l = \frac{2d}{3}$$

$$\delta = l - \frac{D}{2}$$

$$\mathrm{t} = \sin(\frac{\pi}{3})l$$

$$2\delta = \mathrm{d}\left[\frac{4}{3} - \left(\frac{8\phi}{\sqrt{3}\pi}\right)^{\frac{1}{2}}\right] = 1.09 \text{ nm}$$

$$S_x = 2t - D = \mathrm{d}\left[\sqrt{\frac{4}{3}} - \left(\frac{8\phi}{\sqrt{3}\pi}\right)^{\frac{1}{2}}\right] = 0.45 \text{ nm}$$

$$S_y = 3l - D = \mathrm{d}\left[2 - \left(\frac{8\phi}{\sqrt{3}\pi}\right)^{\frac{1}{2}}\right] = 3.5 \text{ nm}$$

$$\gamma = \frac{3l}{2} - D = \mathrm{d}\left[1 - \left(\frac{8\phi}{\sqrt{3}\pi}\right)^{\frac{1}{2}}\right] = -0.10\ nm$$